Flow Visualization and Forces From a Squeeze Film Damper Operating With Natural Air Entrainment

Luis San Andrés
e-mail: lsanandres@mengr.tamu.edu
Mechanical Engineering Department,
Texas A&M University,
College Station, TX 77843

Sergio E. Diaz
e-mail: sdiaz@usb.ve
Departamento de Mecánica,
Universidad Simón Bolivar,
Caracas, Venezuela

Measurements of dynamic film pressures and high-speed photographs of the flow field in an open-ended Squeeze Film Damper (SFD) operating with natural free air entrainment are presented for increasing whirl frequencies (8.33–50 Hz), and a range of feed pressures to 250 kPa (37 psig). The flow conditions range from lubricant starvation (air ingestion) to a fully flooded discharge operation. The test dynamic pressures and video recordings show that air entrainment leads to large and irregular gas fingering and striation patterns. This is a natural phenomenon in SFDs operating with low levels of external pressurization (reduced lubricant through flow rates). Air ingestion and entrapment becomes more prevalent as the whirl frequency raises, and increasing the feed pressure aids little to ameliorate the loss in dynamic forced performance. As a result of the severity of air entrainment, experimentally estimated damping forces decrease steadily as the whirl frequency (operating speed) increases. [DOI: 10.1115/1.1510878]

Introduction

Squeeze film dampers (SFDs) provide force isolation and energy dissipation in high-speed turbomachinery. SFD design, however, remains empirical at best since predictive models derived from Classical Lubrication do not account for the effects of air ingestion; most persistent for operation with low levels of feed pressure and high whirl speeds [1].

Two characteristic squeeze film actions take place in a SFD during a period of journal whirl motion. As the film thickness (h) decreases ($dh/dt<0$, positive squeeze), the lubricant develops hydrodynamic pressures above ambient and proportional to the journal whirl speed. On the other hand, as the local film increases ($dh/dt>0$, negative squeeze) the dynamic film pressure falls below ambient leading either to lubricant cavitation, or to air entrainment if not enough lubricant is available to fill the local gap. Low feed pressures (reduced flow rates), high whirl speeds, and operation with large journal orbital motions (i.e., traversing critical speeds, blade losses or transient vibrations) make imminent the ingestion of air into the damper film lands; thus affecting greatly its ability to generate damping forces [2,3].

Lubricant vapor cavitation, gaseous cavitation and aeration are the three modes of film rupture known in steadily loaded journal bearings [4]. These film rupture types may also occur in dynamically loaded journal bearings and SFDs, albeit showing more complicated flow patterns. In statically loaded journal bearings, as Fig. 1(a) illustrates, the air or vapor cavity occupies a stationary zone, bounded on one side by lubricant (full film) and vented to the gaseous media on the other side (discharge port). However, cyclic (periodic) loading produces ingestion/expulsion of air into/out from the lubricating film [1,2]. The appearance of large and irregular air fingers migrating throughout the bearing clearance is characteristic of this film rupture form; see Fig. 1(b). In some instances, gas bubbles remain trapped within the fluid as the film pressure rises above ambient. Strong flow reversals certainly aggravate air ingestion.

Contributed by the Tribology Division of THE AMERICAN SOCIETY OF MECHANICAL ENGINEERS for presentation at the ASME/STLE Tribology Conference, Cancun, Mexico October 27–30, 2002. Manuscript received by the Tribology Division January 20, 2002 revised manuscript received July 2, 2002. Associate Editor: S. Wu.

Lubricant vapor and gaseous cavitation phenomena differ markedly with the features and ultimate effects of air entrainment. Unfortunately, the technical literature is often misleading and the terms gaseous cavitation and air entrainment are used indiscriminately to describe the phenomena. Mineral lubricants contain dissolved gases with a saturation pressure slightly below ambient pressure. Early, during the negative squeeze action, sub-ambient pressures are achieved and non-condensable gas (air) comes out from solution. This phenomenon is properly referred to as gaseous cavitation. In degassed lubricants, the pressure continues to fall and oil vaporization (vapor cavitation) may occur. However, when the film clearance connects to a large gaseous plenum, air is easily drawn into the film lands by the suction generated as the local clearance "stretches."

Cole and Hughes [5] report visual observations of film extent and gaseous cavitation in dynamically loaded journal bearings. By extension, cavitation in SFDs has since been considered to be of a similar type. White [6] questions this rationale in lieu of flow visualizations conducted on a test SFD that revealed finger-like cavities, growing and shrinking during a journal whirl cycle. Marsh [7], referring to the same experimental results, estimated SFD forces that are just a fraction, 5 percent to 25 percent in magnitude, of the forces predicted using Classical Lubrication Theory. Bansal and Hibner [8] present further experimental results that evidence the inadequacy of Reynolds equation to predict damper reaction forces. The authors speculate that the deviation is due to fluid compressibility caused by sub-atmospheric pressures liberating dissolved gases and creating a two-phase fluid. Walton et al. [9] used high-speed photography to reveal flow patterns in a SFD executing circular centered orbits, and again note severe discrepancies with accepted lubrication theory predictions.

Zeidan and Vance [3] identified five regimes of cavitation in a SFD according to its operating conditions, and with air entrainment occurring at large amplitudes of journal motion. Flow visualization revealed the formation of a bubbly mixture, with air bubbles persisting even in above ambient pressure zones. Radial and tangential forces estimated from the measured dynamic pressures show a nonlinear characteristic akin to that of a softening spring. Diaz and San Andrés [2,10–12] have conducted the most comprehensive experiments to date, and report the evolution of film pressures during a period of journal motion for increasing

 Copyright © 2003 by ASME

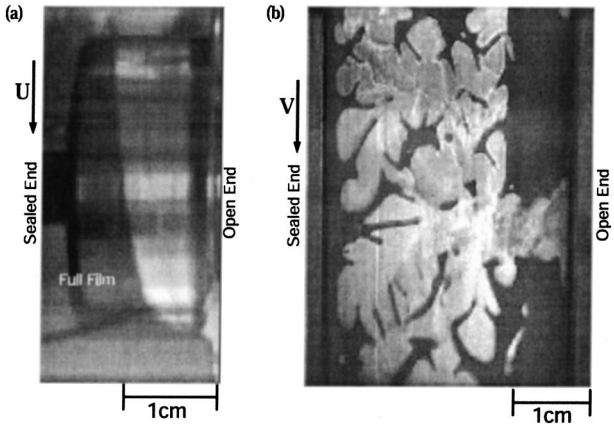

Fig. 1 (*a*) Stationary aerated cavity in a journal bearing; (*b*) Squeeze film flow of an open-ended SFD subject to air entrainment (window span of 30°). U and V denote the journal rotational speed and whirl speed, respectively.

contents of air in a controlled lubricant mixture (from pure oil to 100 percent air). A (synchronous) period-averaging scheme filtered the random fluctuations and spikes in the recorded pressures. The measurements show decreasing peak-to-peak pressures and reduced SFD reaction forces for increasing air contents in the lubricant. The authors recently advanced a predictive analytical/empirical model that correlates well with their measurements [2].

This paper presents measurements of dynamic film pressures and high-speed photographs (video recordings) of the flow field in a SFD operating with natural free air entrainment. The experiments were conducted in an open-ended damper with moderately large journal orbital motions ($\varepsilon_c \rightarrow 0.55-0.75$) and increasing whirl frequencies (8.33–50 Hz).

Experimental Setup

The experiments were conducted on a circular-centered orbit SFD operating with one end vented to ambient [10]. Figure 2 depicts a schematic view of the test rig, whose open-end provides a natural path for air entrainment into the squeeze film zone. The damper journal and its ball bearing are mounted on a rigid shaft with an eccentric collar that produces the circular orbits at a whirl frequency synchronous with the shaft rotational speed. The damper journal length (L), diameter (D) and radial clearance (C) are 31.1 mm, 129.4 mm, and 0.254 mm, respectively. The nominal orbit radius (e) is 0.180 mm ($e/C=0.71$). The uncertainty in the damper dimensions including its clearance and orbit radius is ± 0.0127 mm (± 0.5 mil).

An ISO VG 68 lubricant was employed in the tests. The oil has a density of 877 kg/m^3 and viscosity of 156.5 cPs at 22.4°C and 56.9 cPs at 40°C, respectively. A DC motor driven gear pump delivers oil to the damper through the inlet holes. A digital flow meter displays the amount of oil fed into the damper. The transparent Plexiglas damper housing, see Fig. 2, contains four strain gauge (absolute) pressure transducers located at two axial planes (one at $Z_1=5.6$ mm and three at $Z_2=16.7$ mm from the sealed end) and three circumferential positions (0 deg, 150 deg, and 210 deg). K-type thermocouples record the lubricant inlet and outlet temperatures. A T-type thermocouple, flush with the inner diameter of the housing, senses the film temperature at the Z_2 plane. Eddy current (non-contacting) displacement transducers measure the journal displacements in two orthogonal planes. The motion signals are used to verify the journal circular motion, establish the orbit centering, and provide a direct estimation of the film thickness.

Journal displacements and film dynamic pressures are acquired with a dedicated DAQ system and stored in a PC. Temperatures, feed and discharge static pressures, flow rate and electrical power are recorded manually from the instrumentation and logged into the DAQ software. A high-speed digital camera with a recording capacity up to 3000 frames/s was used to obtain photographs of the flow patterns.

Experimental Procedure

Measurements of film dynamic pressures, journal motion, film temperature, and inlet and outlet port conditions were performed for gradual increments of the oil flow rate while maintaining a constant rotor speed from 500 to 3000 rpm, with increments of 500 rpm. The lubricant flow rate was increased discretely (~0.1 *l*/min) until the return auxiliary pump was not able to evacuate all the lubricant, and the discharge plenum started to flood (typically beyond 0.8 *l*/min). At the highest flow rate, the main pump was

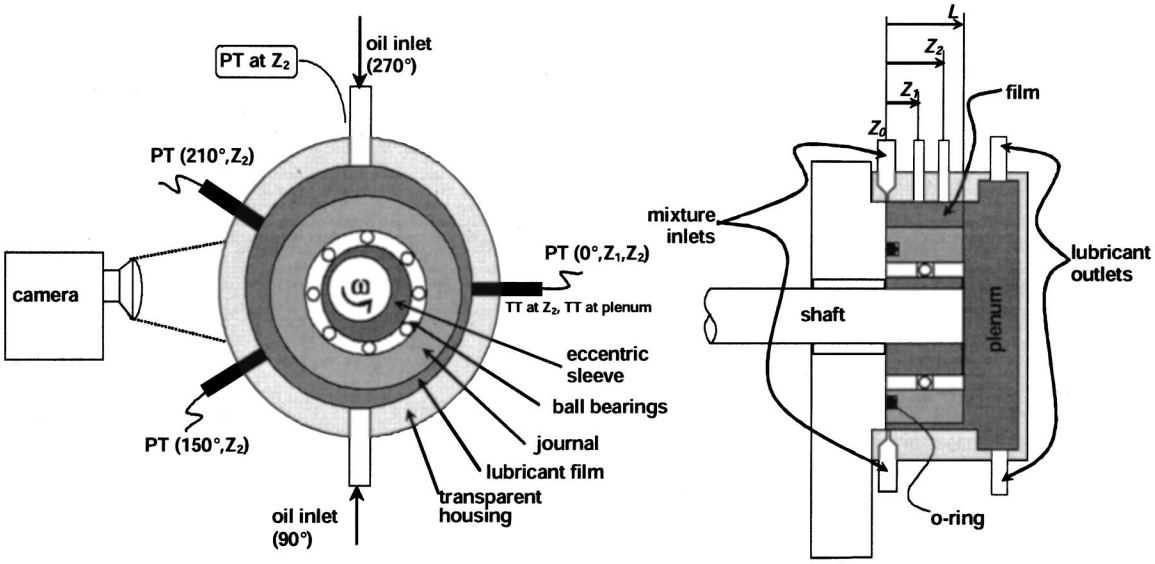

Fig. 2 Schematic view of test rig and instrumentation ($L=31.1$ mm (1.22 in), $D=129.3$ mm (5.10 in), $C=0.254$ mm (0.010 in), $Z_1=5.6$ mm (0.22 in), $Z_2=16.7$ mm (0.66 in), $Z_3=37.1$ mm (1.46 in), PP: Displacement sensor, PT: pressure transducer, TT: Thermocouple, PG: pressure gauge).

turned-off momentarily and an auxiliary pump evacuated lubricant from the discharge plenum. Then, the main pump was turned-on again, and the video recording triggered once a uniform flow was attained and the squeeze film flow pattern evolved. The movie recording stopped before having a semi-flooded discharge condition.

Test conditions included six speeds (500 to 3000 rpm) and nine supply pressures (feed flow rates). Static measurements; namely rotor speed, lubricant flow rate and feed pressure, film and inlet/outlet port temperatures, and the motor drive power, were recorded manually. The DAQ sampling rate for displacements and dynamic pressures was set to 1000 samples/s with 2048 data points/record in each experiment.

Estimates of the fluctuations on the instantaneous peak-to-peak (*p-p*) pressure were determined by finding the lowest ever and highest ever magnitudes over the elapsed testing time. Period averaged orbit amplitudes in the horizontal (X) and vertical (Y) directions, as well as orbit offsets, followed a similar procedure from estimation of the maximum and minimum journal displacements in each direction.

The SFD is circumferentially symmetric, and thus, the dynamic pressure field "rotates" at the same speed as the journal whirl frequency. Diaz and San Andrés [10–12] detail the time dependency of the measured variables and the temporal fluctuations associated with bubbly lubricant mixtures. Presently, dynamic pressure profiles recorded during 14 full periods of journal motion are period averaged to render smooth fields characteristic of a full cycle of journal motion. The instrumentation uncertainty is much smaller that the uncertainty arising from the dynamic variations in the recorded film pressure and journal displacements [10].

Digital films were recorded at 500 frames/s in all experiments. White tissue paper wrapped around the apparatus provided a suitable lighted environment and reduced the sharp reflection of the intense light on the damper surface. The camera lens was adjusted to span a window 30 deg wide in the circumferential direction and the whole damper axial length. The lubricant was colored with an inert dark-blue powder dye to enhance the contrast between the lubricant and the ingested air fingers. The still photographs synchronized with the journal displacements and the dynamic pressure measurements evidence characteristic flow patterns.

Experimental Results

In each test, the shaft speed was maintained as the lubricant supply pressure increased to span feed conditions from nearly no flow (starvation) to full through flow rates at high feed pressures. Note that significant variations of the lubricant temperature at the inlet port were recorded during the numerous tests (from 25°C to 35°C). Thus, the measurements evidence an inlet lubricant viscosity determined by the testing time. Warm lubricant coming out from the damper mixed with the oil in the sump and elevated its temperature. Each experiment, spanning feed pressures from low to high magnitudes, took about 20–25 minutes for completion.

Table 1 sums the test conditions and main static measurements; namely rotor speed, lubricant flow rate and feed pressure, film and inlet/outlet port temperatures. In most experiments the lubricant temperature at the inlet and outlet ports shows a difference of only 2°C, while the film temperature at the Z_2 plane could be 10°C higher than the inlet temperature. The results thus show low heat convection rates for the lubricant since the flow rates were rather small at the onset of each set of experiments. Thus, as a set of measurements proceeded, the journal and damper warmed up rapidly, and the film temperature recorded corresponds to that of the housing and not the actual one within the fluid film. The damper and journal were already hot once the higher flows were achieved, and the lubricant flowing through the film was unable to remove the dissipated heat during the remaining test time.

Film Dynamic Pressures and Flow Visualization. Air naturally entrained into the damper clearance for flow conditions not flooding the damper discharge plenum. Fig. 3 shows measured

Table 1 Test conditions: whirl speed, lubricant inlet flow rate, feed pressure, temperatures, and orbit radius (e/C).

Oil Inlet Flow	Gauge Feed Pressure (P)		Temperatures Inlet	Plane Z_2	Outlet	e/C
lt/min	psi	kPa	°C	°C	°C	
500 rpm						
0.07	5	34.5	22.2	24.4	23.9	0.71
0.21	12	82.7	22.2	31.7	25.0	0.64
0.31	16	110.2	23.3	33.9	25.6	0.64
0.42	18	124.0	26.1	36.7	27.2	0.64
0.52	22	151.6	26.7	36.7	28.9	0.64
0.62	26	179.1	26.7	36.7	28.3	0.64
1500 rpm						
0.08	5	34.5	22.2	26.1	23.9	0.69
0.11	8	55.1	22.2	28.9	23.9	0.65
0.21	12	82.7	22.8	31.1	25.6	0.64
0.29	16	110.2	23.9	33.3	26.1	0.61
0.39	19	130.9	24.4	36.7	27.2	0.60
0.49	23	158.5	26.1	36.5	27.8	0.59
0.59	26	179.1	27.2	36.1	28.3	0.59
0.79	31	213.6	27.8	37.2	29.4	0.58
3000 rpm						
0.08	6	41.3	22.2	31.7	24.4	0.70
0.21	12	82.7	22.8	33.3	26.1	0.68
0.30	16	110.2	23.9	34.4	26.7	0.66
0.40	20	137.8	25.6	36.1	26.1	0.63
0.50	22	151.6	26.7	36.7	28.3	0.63
0.60	25	172.2	27.8	37.2	29.4	0.63
0.69	28	192.9	27.8	37.8	30.0	0.64
0.80	31	213.6	28.3	38.3	30.0	0.63
0.91	33	227.4	28.3	38.3	30.6	0.60

Lubricant viscosity vs. temperature: $\mu = \mu_{ref} e^{\alpha(T-T_{ref})}$, where $\mu_{ref} = 156.5$ cPs, $T_{ref} = 22.4°$ C, and $\alpha = -0.057$/°C.

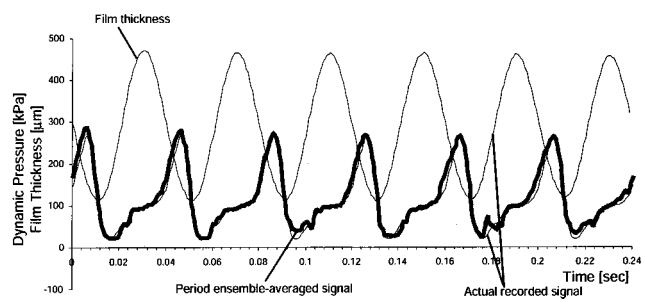

Fig. 3 Film dynamic pressure (210°, Z_2) and period averaged pressure, and film thickness versus time for test at 1500 rpm and 55 kPa (8 psi) gauge feed pressure. Period of motion = 40 ms.

film pressures at (210 deg, Z_2) and journal X-motion at 1500 rpm (25 Hz) and feed pressure equal to 55 kPa (8 psig). The pressure signals have been shifted by known phase angles relative to the journal displacement signal. Note the fluctuating and intermittent behavior of the film pressures with sudden pressure spikes and

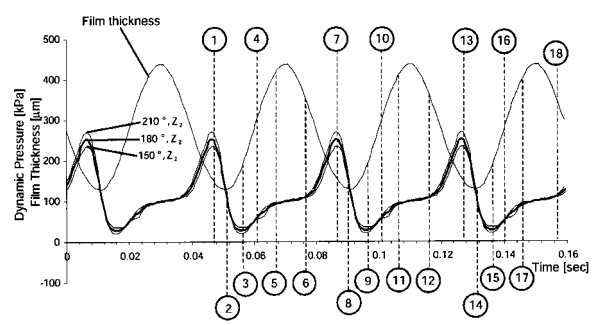

Fig. 4 Period-average film pressures at (210°, Z_2), (150°, Z_2) and (180°, Z_2) and film thickness versus time for test at 1500 rpm and 55 kPa (8 psig) gauge feed pressure. Numbered circles relate to photographs of flow depicted in Fig. 5.

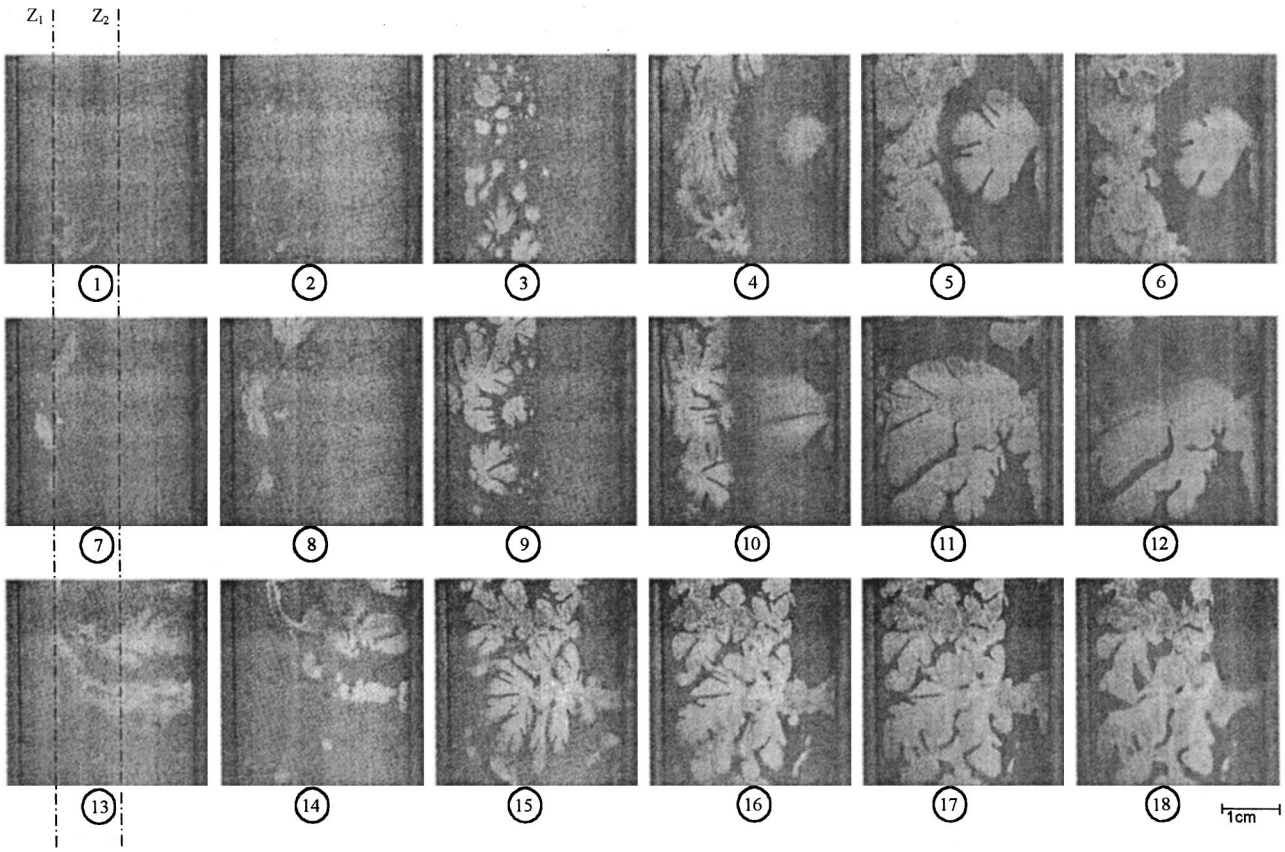

Fig. 5 Photographs of flow field in SFD (30° span) at key instances of journal motion (see Fig. 4). Frames in same column correspond to the same relative instant within a period of motion. Frames 1–6 correspond to 1st period, 7–12 to 2nd period, and 13–18 to 3rd period.

variations of the peak-to-peak (*p-p*) pressure between consecutive periods of journal motion. Furthermore, a nearly uniform pressure zone evolves around the location of maximum film thickness with sub-ambient pressures occurring on each half-period of (negative) squeeze motion. Despite the random irregularities there is an apparent periodicity as revealed by the (synchronous speed) period averaged pressure[1] also displayed in the Figure.

Figure 4 shows characteristic (period averaged) dynamic absolute pressure profiles at (150 deg, Z_2), (210 deg, Z_2) and (180 deg, Z_2) and the *X*-journal motion for a test at 1500 rpm and 55 kPa (8 psig) feed pressure. The dynamic pressures at 150 deg and 210 deg are shifted by phase angles with respect to the displacement signal. The procedure allows direct correlation of the generated dynamic pressures and the instantaneous journal displacement. In the discussion, the dynamic film pressure at the camera location (180 deg, Z_2) is considered as the simple average of the pressures recorded at 150 deg and 210 deg. Note the similarity of the (synchronous speed) period-averaged pressure profiles obtained at the different angular locations. The experimental results thus demonstrate that the multiple period-averaged film pressure does rotate around the journal in synchronicity with the shaft speed.

Numbered circles in Fig. 4 correspond to photographs of the flow field at key instances within three periods of journal motion and displayed in Figure 5. The period of motion is 0.040 s at 1500 rpm (25 Hz). The photographs in the same row correspond to a single period of journal motion, namely 1–6 (1st period), 7–12 (2nd period) and 13–18 (3rd period). The picture frames in the same column refer to the flow pattern observed at about the same instant of time relative to a journal period of motion.[2] From left to right, the journal goes through the minimum film thickness at positions 2, 8, and 14; then the film thickness increases ($dh/dt > 0$, negative squeeze) to frames (5, 11, 17), and the local film decreases ($dh/dt < 0$, positive squeeze) in frames (6–7), (12–13), and (18), respectively. Peak dynamic pressures occur at frames (1), (7), and (13) just before the local minimum film thickness.

In general, the photographs evidence air ingestion as large irregular finger-like cavities moving from the open plenum towards the SFD sealed end, in particular at those instances where the film rate of change (dh/dt) is maximum as depicted in frames (4–5), (10–11), and (16–17). The large air striations (at nearly ambient pressure) migrate rapidly into the film lands. The large zones of air entrainment persist even at the beginning of the positive squeeze zone, i.e. while the local film decreases ($dh/dt < 0$), as seen in frames (6), (12) and (18). However, most of the air is expelled within a fraction of the journal periodical motion while the film pressure builds up rapidly above ambient, as frames (1), (7), and (13) evidence. The drop from peak film pressure to the sub ambient value is also rapid; and frames (2), (8), and (14) show the beginning of air ingestion and, in some instances, pressures near zero absolute.[3]

A complete analysis of the flow patterns recorded for several journal periods of motion demonstrates that no more than two consecutive periods of motion show similar flow patterns at each

[1]Diaz and San Andrés [10,12] earlier experiments demonstrated the striking similarity between the pressure profiles resulting from air entrainment and those obtained with a homogeneous (controlled) bubbly mixture.

[2]The authors offer composite digital movies of the flow field and pressures for most tests. The interested reader should contact the authors and request the information available in CD format.

[3]The calibration of the offset for the (absolute) pressure sensors proved difficult, changing over time due to heating of the sensor. The small values of negative pressures reported are probably due to the thermally induced drift.

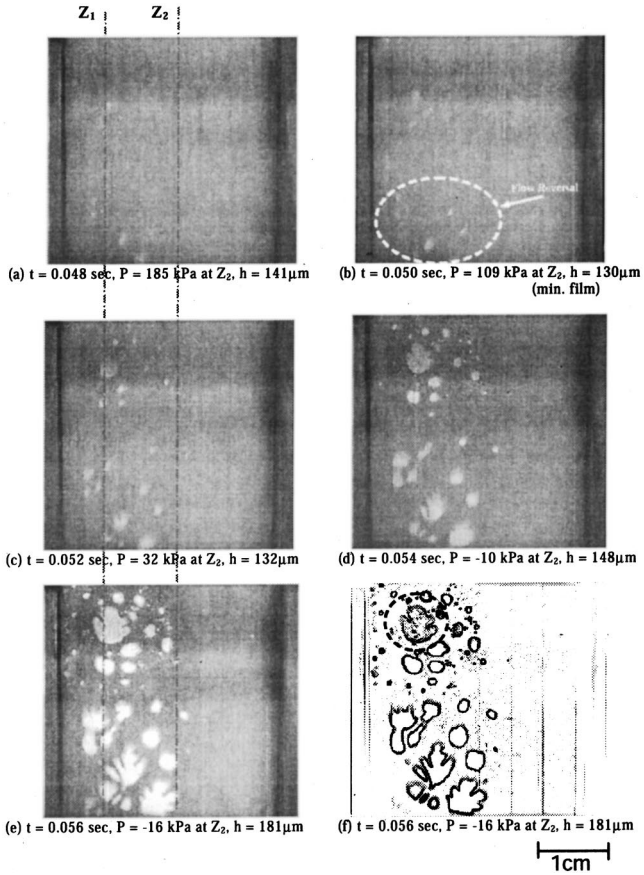

Fig. 6 Series of flow images depicting bubble growth within lubricant film. Tests at 1500 rpm (25 Hz) and 55 kPa (8 psi) gauge feed pressure. Period of motion=40 ms.

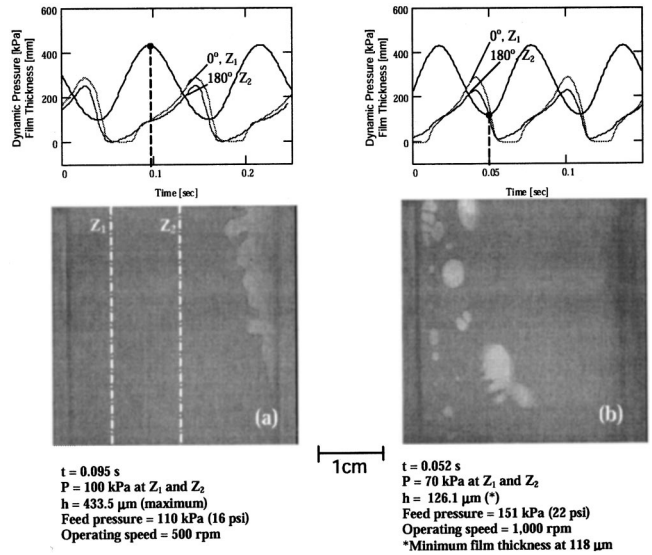

Fig. 7 Film dynamic pressures and film thickness and flow photographs at (*a*) 110 kPa/500 rpm, (*b*) 151 kPa/1,000 rpm

relative instant of motion. For example, frames 13 and 14 in Fig. 5 show zones of entrapped air cavities able to withstand the maximum pressure, and remaining even as the film thickness reaches a minimum about 210 kPa and 130 μm, respectively (also refer to circles 13 and 14 in Fig. 4). Thus, the amount of air entrained differs in each period of motion, and its persistence in the high-pressure region leads to pressure spikes as the local film thickness decreases. The large striations and fingers ingested into the damper lands obviously contain air drawn from the vented end of the test damper. The contents of the minute rounded-like cavities could be mostly a mixture of vapor lubricant and dissolved gases, in lieu of the low dynamic pressures recorded.

Figure 6 shows a series of photographs displaying the inception and persistence of local lubricant cavitation while the pressure drops from peak to sub ambient values. The time instants and pressures (see captions) correspond to the pressure profile shown in Fig. 4. Frame (*a*) shows some cavities that have persisted in the high-pressure zone. Next in frame (*b*), a flow reversal occurs at the instant of minimum film thickness and local pressure just below ambient [circle # 2, Fig. 4]. As the film thickness begins to increase ($dh/dt>0$), frames (*c*) and (*d*) show the growth of the cavity volumes and the emergence of others into the visual field. Most likely, the small size cavities contain a mix of lubricant vapor and air that comes out of solution. As the film thickness locally increases and the pressure reduces, their volume grows and becomes visible. Frame (*e*) at the instant of lowest recorded pressure (near zero absolute) displays enlarged cavities, resulting from the merging (coalescence) with others. Note that there is still a large portion of the film covered with lubricant, and (perhaps) able to sustain some tension.

Frame (*f*) in Fig. 6 depicts a digitally enhanced version of frame (*e*) (also frame 3 in Fig. 5). The gas cavity enclosed within a circle shows some small ''inclusions.'' The digital image processing displays their edges, thus revealing its liquid content, otherwise they would diffuse within the enclosing cavities. The liquid drops could be attached to the bearing or journal surfaces, or suspended within the larger irregular gas (air) cavity. The presence of these liquid drops, as remnants of the full film of lubricant, may be related to the surface finish of the damper housing and journal.

Figure 7 depicts other measurements of journal motion and film pressure versus time, and flow pictures for two feed pressures and rotor speed conditions: (*a*) 110 kPa (16 psig) and 500 rpm, and (*b*) 151 kPa (22 psig) and 1000 rpm. In (*a*), note that a larger feed pressure helps to reduce the extent of air ingestion (compare with frames 5, 11, and 17 in Fig. 5). In (*b*), even a larger feed pressure cannot prevent the onset of lubricant vaporization for operation at higher rotor speeds (compare with frames 2, 8, and 14 in Fig. 5). The flat portion in the pressure profiles recorded at Z_1 is at near zero absolute pointing to a zone of lubricant vaporization.

Figure 8 displays the multiple-period (synchronous speed) averaged film pressures for increasing journal speeds at the different locations of measurement and for a range of feed pressures. The graphs on the left and right columns correspond to axial locations Z_1 and Z_2, respectively. The test results at the lowest speeds (500 and 1000 rpm) show a marked difference in the pressure profiles for low and high feed pressures. At low feed pressures, the pressure field shows a typical zone of uniform pressure at ambient conditions and relatively small time regions where the pressure rapidly changes, either towards a peak positive value or sub ambient towards zero absolute. In these measurements, air ingestion prevails. On the other hand, increments in the feed pressure (larger flow rates) reduce air ingestion and the pressure field evolves continuously from low to high to low magnitudes; and in some instances developing vapor lubricant cavitation, particularly at axial location Z_1. The measurements at the highest speed (3000 rpm) show dynamic pressures typical of air ingestion in spite of the increases in feed pressure (larger through flow rate).

Figure 9 depicts large air fingering even for a relatively high-feed pressure (193 kPa [28 psig]). The measured pressure profiles closely resemble those obtained earlier with a controlled bubbly mixture [10]. Thus, large lubricant flow rates (high feed pressure) and low operating speeds delay air entrainment in SFD operation. High inlet pressures are desirable although the cost and size of such an arrangement is not affordable in practical applications.

The repeatability of the measurements was enhanced as the

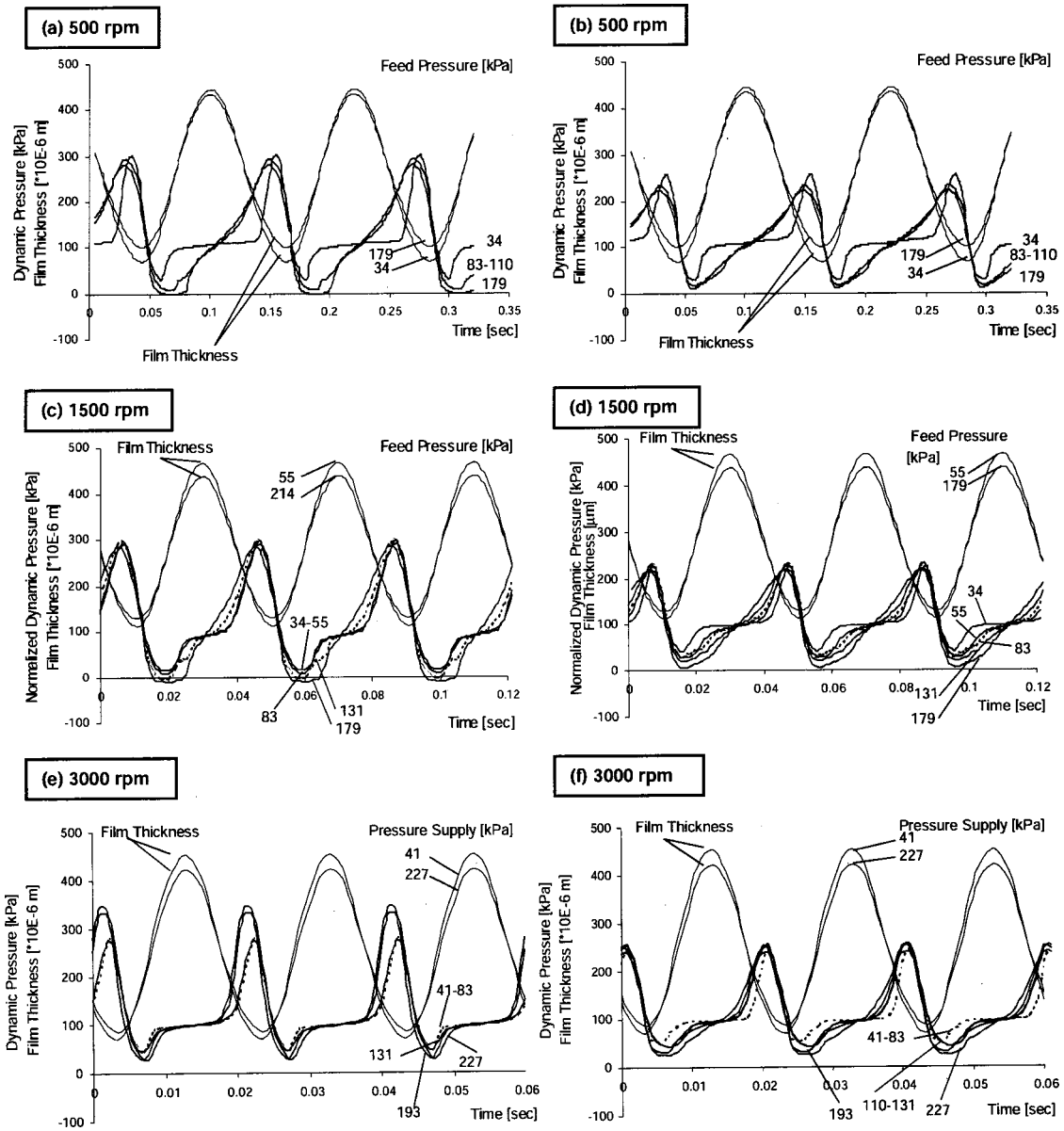

Fig. 8 Film dynamic pressures and film thickness versus time for all tests. Feed pressure/speed varies. Left: Z_1 and right: Z_2 planes.

lubricant feed pressure increased. At low feed pressures the fluctuations in the measured dynamic pressures and journal displacements are significant due to the random distribution of the ingested air fingers within the damper lands.

Peak Dynamic Pressures and Estimated Film Forces. Figure 10 shows the recorded peak-peak (*p-p*) dynamic film pressures versus feed pressures for speeds of 500, 1500, and 3000 rpm. Figure 11 displays similar results as a function of the rotor speed and ranges of feed pressures. The overall temporal variation (first order uncertainty) in the *p-p* pressures from (no less than) 16 periods of motion at the Z_1 and Z_2 planes are ± 4 percent at 500 rpm, ± 12 percent at 1500 rpm and ± 23 percent at 3000 rpm, respectively. The analysis of the recorded test data then shows that as the operating speed increases, the fluctuations in the *p-p* dynamic pressures increase since air entrainment becomes more severe. The *p-p* pressures recorded at the Z_1 plane (Fig. 11(*a*)) remain fairly constant with respect to variations in the feed pressure and speed. However, the *p-p* pressures recorded at the Z_2 plane (Fig. 11(*b*)) show a somewhat irregular behavior as the speed increases. Most importantly, note that the *p-p* pressures remain relatively constant for increasing feed pressures and rotor speeds. This apparently contradictory behavior is probably related to the drop in lubricant viscosity as testing progressed, and due to the inlet temperature raise and hot journal and bearing surfaces.

The squeeze film forces $(f_r, f_t)_{(Z)}$ per unit length in the radial and tangential directions are estimated from numerical integration of the measured dynamic pressures over a period of journal motion. The procedure also gives the ensemble radial and tangential forces (f_r, f_t) by averaging the forces obtained from the pressures at the different angular locations in the same axial plane.

Figure 12 depicts the film forces versus the feed pressure at three operating speeds and at the axial locations of measurement. The experiments at 500 rpm reveal an increase in tangential (damping) forces $(f_{t(Z_2)})$ towards an asymptotic value, and decreasing radial forces $(f_{t(Z_2)})$ as the feed pressure rises. At 1500 rpm, the tangential force grows for the range of the feed pressures, while the radial force remains relatively constant. The same rationale follows at 3000 rpm (50 Hz), although the radial force at

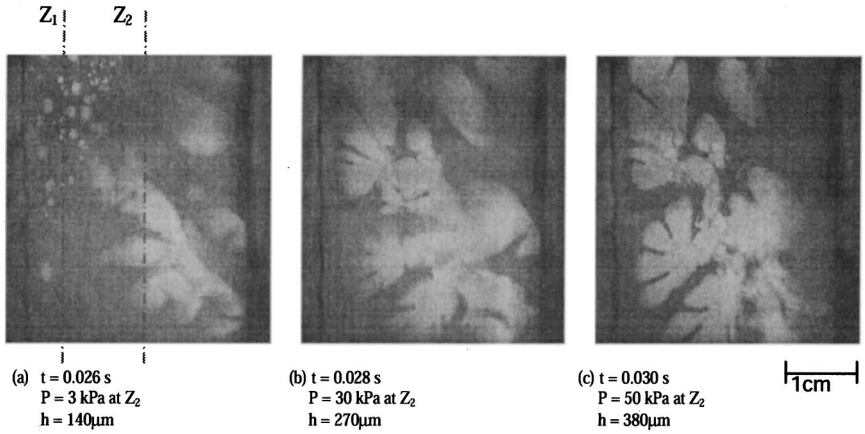

Fig. 9 Photographs of flow field for a test at 1500 rpm and feed pressure 193 kPa (28 psi). Elapsed time for photographs is 2 ms (Period=40 ms).

plane Z_1 appears to grow slightly, probably due to the occurrence of vapor cavitation. Thus, increasing the feed pressure causes flooding of the squeeze film region and diminishes the effects of air entrainment (lubricant cavitation as well). Note that the average forces derived from pressures recorded at three angular locations of measurement (Z_2) do not differ much from the individual forces at each circumferential location. Thus, the measurements indicate the period-average pressure field is representative of the dynamic behavior at all circumferential locations.

Most importantly, however, the forces derived from the experimental film pressures decrease rapidly as the journal speed (whirl frequency) increases. Figure 13 shows the film forces, radial and tangential, versus journal speed for the range of feed pressures in the tests (at Z_2 plane). Note that the radial forces are relatively

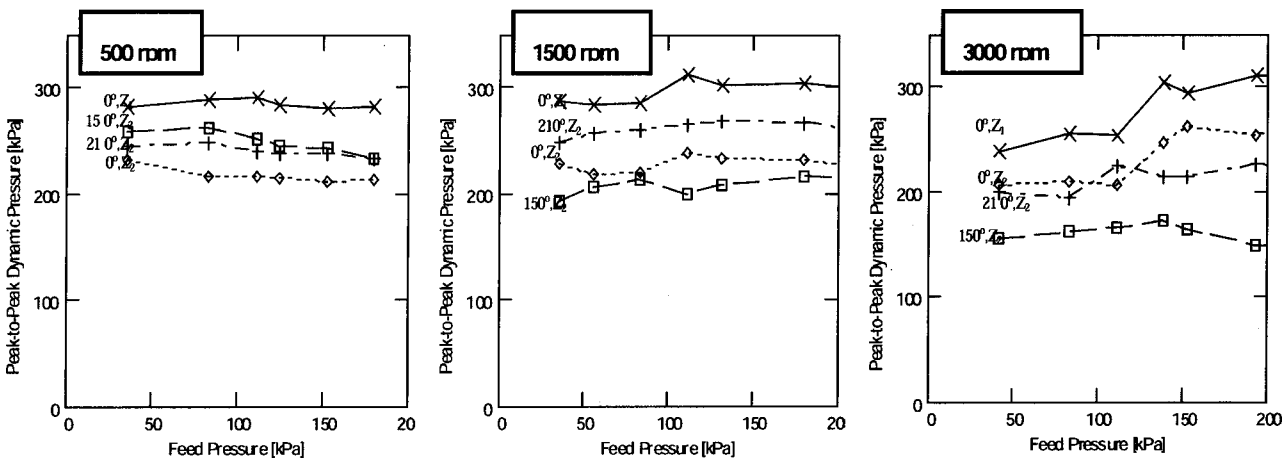

Fig. 10 Peak-to-peak dynamic film pressures versus feed pressure for tests at 500, 1500, and 3000 rpm (Two axial locations of measurement).

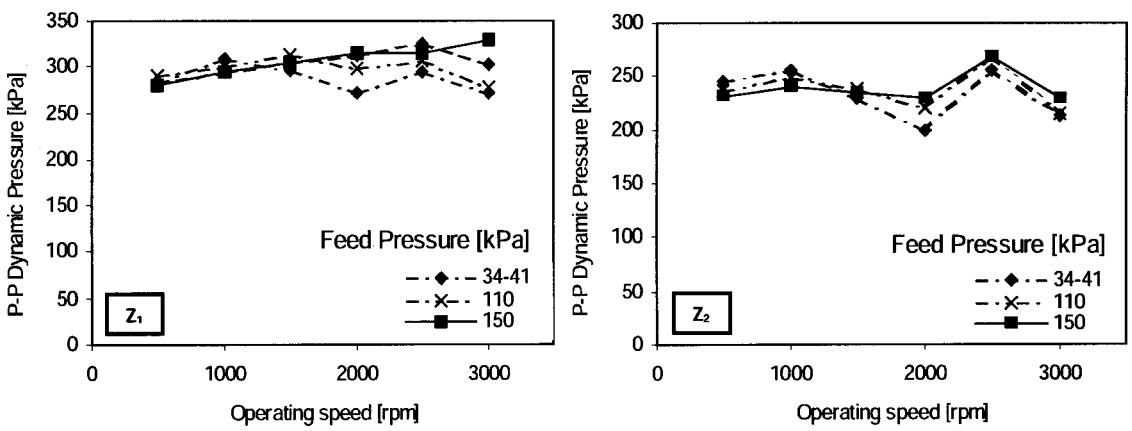

Fig. 11 Peak-to-peak dynamic film pressures versus journal speed for range of feed pressures. Two axial locations of measurement noted.

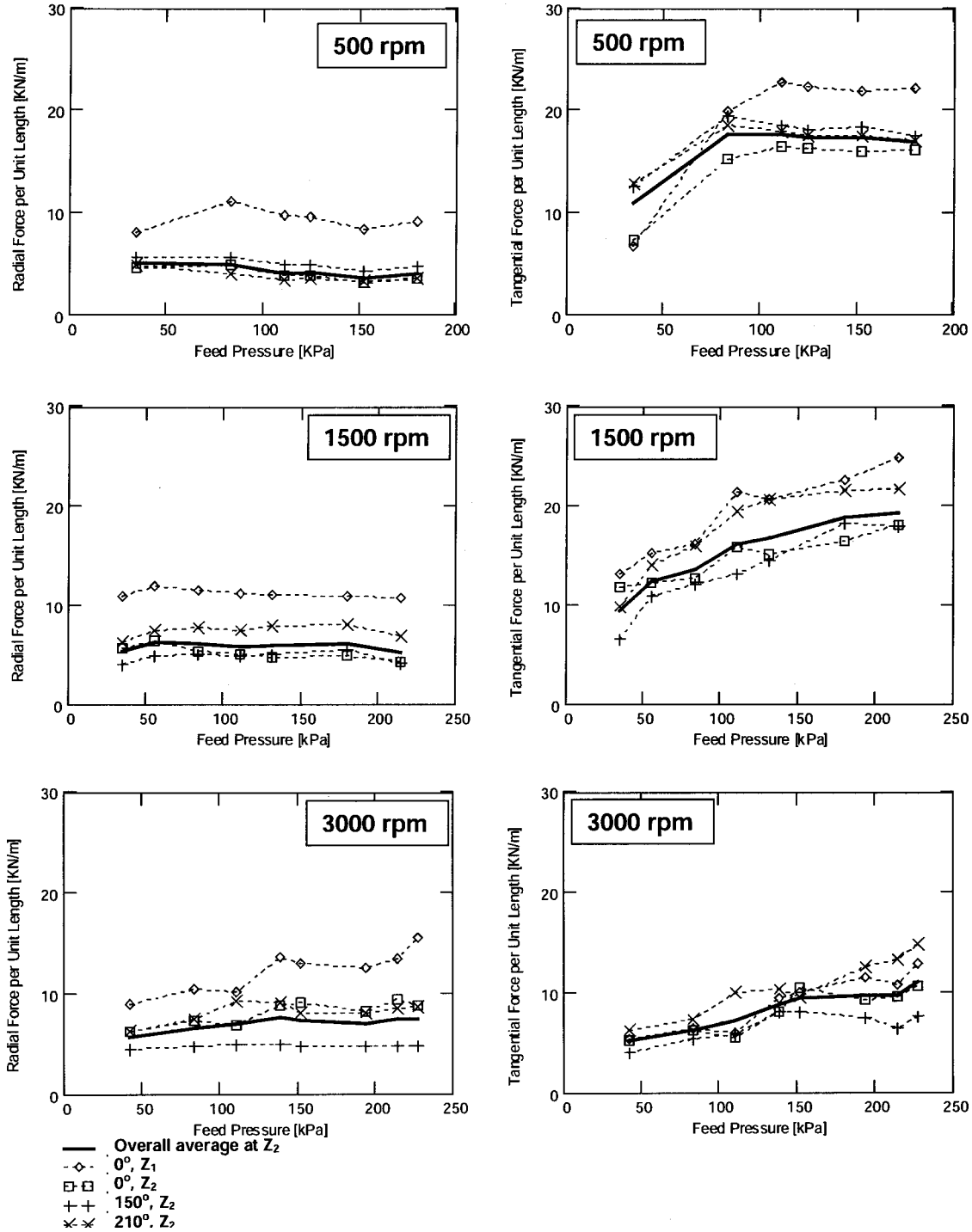

Fig. 12 Estimated radial and tangential damper forces/unit length versus feed pressures. Two axial locations of measurement noted.

smaller than the tangential damping forces at low speeds. However, the damping (tangential) forces drop rapidly as the whirl frequency increases. This finding opposes analytical predictions based on Classical Lubrication Theory[4v] and evidences the paramount effect of air entrainment on degrading the SFD dynamic forced performance. Comparisons with predictions derived from the model given in [2] will be advanced in a future publication.

Conclusions

Experiments were conducted on a controlled orbit test SFD operating with an end plenum vented to ambient conditions. Measurements of the dynamic film pressures at two axial planes and journal motion were performed for increasing journal speeds to 3000 rpm and a range of feed pressures to 250 kPa (37 psig).

[4]Fluid film reaction forces increasing linearly with whirl frequency are derived from Classical Theory. The present measurements and others given in [2,3,6,10,11,12] show the opposite behavior due to the air ingestion and entrapment into the film lands.

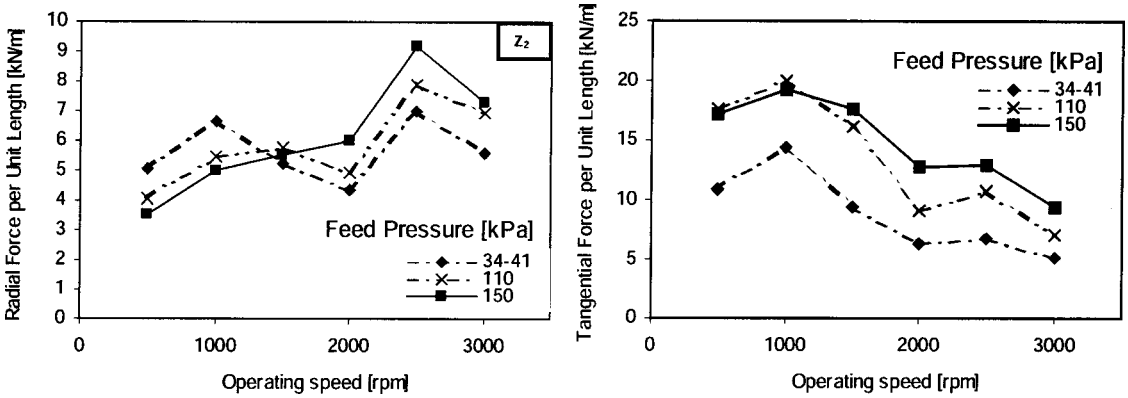

Fig. 13 Estimated radial and tangential damper forces/unit length versus journal speed at Z_2 plane

High-speed video recordings at selected operating conditions revealed the unique features of the flow field within the SFD. Digital movie clips showing the flow field and pressure and motion measurements are available for further analysis.

The experiments show that air entrainment leading to the formation of irregular gas fingering and striation patterns is a natural phenomenon in SFDs operating with low levels of external pressurization (low lubricant through flow rates). Operation at high whirl frequencies always shows this pervasive behavior even for large feed pressures. SFD film damping (tangential) forces decrease as the journal whirl frequency grows.

Air ingestion and entrapment becomes more prevalent as the whirl frequency grows, and increasing the feed pressure aids little to ameliorate the loss in dynamic forced performance. The conclusions derived, however, must be taken with caution since in the experiments, the lubricant heated rapidly over the long test time spanning the range from low to high feed pressures. Thus, the experimentally derived film forces include the (yet not quantifiable) effect of a decreasing viscosity as the feed pressure increases. Controlled temperature experiments are presently being conducted.

Acknowledgments

The support of NSF and the Turbomachinery Research Consortium are gratefully acknowledged. Thanks to students Leonardo Urbiola, Nijesh Jayakar and Jack Charles for conducting the measurements and preparing the digital movies. We also recognize the continued interest from Dr. Jorn Larsen-Basse at NSF.

Nomenclature

C = SFD nominal radial clearance [0.254 mm]
D = journal diameter [129.4 mm]
e = nominal orbit radius [0.180 mm]
f_r, f_t = radial and tangential force per unit length at axial location Z_j
h = local film thickness [m]
L = SFD journal length [31.1 mm]
P = film dynamic pressure [kPa]
r, t = radial and tangential coordinates
T = temperature [°C]
Z_j = axial location of measurements. Z_1 (5.6 mm), Z_2 (16.7 mm)
ε = e/C, dimensionless orbit radius
θ = circumferential coordinates [rad]
μ = lubricant viscosity [Pa.s]
ω = journal whirl frequency [rad/sec]

References

[1] San Andrés, 2000, "Squeeze Film Dampers—Design and Operating Issues," *Class Notes on Modern Lubrication*, Texas A&M University, College Station, TX.
[2] Diaz, S., and San Andrés, L., 2001, "A Model for Squeeze Film Dampers Operating with Air Entrainment and Validation with Experiments," ASME J. Tribol., **123**(1), pp. 125–133.
[3] Zeidan, F. Y., and Vance, J. M., 1990, "Cavitation Regimes in Squeeze Film Dampers and Their Effect on the Pressure Distribution," STLE Tribol. Trans., **33**, pp. 447–453.
[4] Dowson, D., and Taylor, M. 1974, "Fundamental Aspects of Cavitation in Bearings," *Proceedings of the 1st Leeds-Lyon Symposium on Tribology*, University of Leeds, England, pp. 15–28.
[5] Cole, J. A., and Hughes, C. J., 1957, "Visual Study of Film Extent in Dynamically Loaded Complete Journal Bearings," Proc. Lub. Wear Conf., pp. 147–149.
[6] White, D. C., 1970, "Squeeze Film Journal Bearings," Ph. D. Dissertation, Cambridge University.
[7] Marsh, H., 1974, "Cavitation in Dynamically Loaded Journal Bearings," *Proceedings of the 1st Leeds-Lyon Symposium on Tribology*, University of Leeds, England, pp. 91–95.
[8] Bansal, P. N., and Hibner, D. H., 1978, "Experimental and Analytical Investigation of Squeeze Film Bearing Damper Forces Induced by Offset Circular Whirl Orbits," ASME J. Mech. Des., **100**, pp. 549–557.
[9] Walton, J., Walowit, E., Zorzi, E., and Schrand, J., 1987, "Experimental Observation of Cavitating Squeeze Film Dampers," ASME J. Tribol., **109**, pp. 290–295.
[10] Diaz, S., and San Andrés, L., 1997, "Measurements of Pressure in a Squeeze Film Damper with an Air/Oil Bubbly Mixture," STLE Tribol. Trans., **41**(2), pp. 282–288.
[11] Diaz, S., and San Andrés, L., 1998, "Reduction of the Dynamic Load Capacity in a Squeeze Film Damper Operating with a Bubbly Mixture," ASME J. Eng. Gas Turbines Power, **121**, pp. 703–709.
[12] Diaz, S., and San Andrés, L., 2001, "Air Entrainment Versus Lubricant Vaporization in Squeeze Film Dampers," ASME J. Eng. Gas Turbines and Power, **123**(4), pp. 871–877.